THE JOURNAL OF PHYSICAL CHEMISTRY B

Article

pubs.acs.org/JPCB

Molecular Simulation and Experimental Study of CO_2 Absorption in Ionic Liquid Reverse Micelle

Wei Shi,*[†,‡,§] Lei Hong,[†,‡] Krishnan Damodaran,[⊥] Hunaid B. Nulwala,[#] and David R. Luebke[†]

[†]U.S. Department of Energy, National Energy Technology Laboratory, Pittsburgh, Pennsylvania 15236, United States

[‡]URS Corporation, South Park, Pennsylvania 15129, United States

[§]Department of Chemical and Petroleum Engineering, University of Pittsburgh, Pittsburgh, Pennsylvania 15261, United States

[⊥]Department of Chemistry, University of Pittsburgh, Pittsburgh, Pennsylvania 15260, United States

[#]Department of Chemistry, Carnegie Mellon University, Pittsburgh, Pennsylvania 15213, United States

Supporting Information

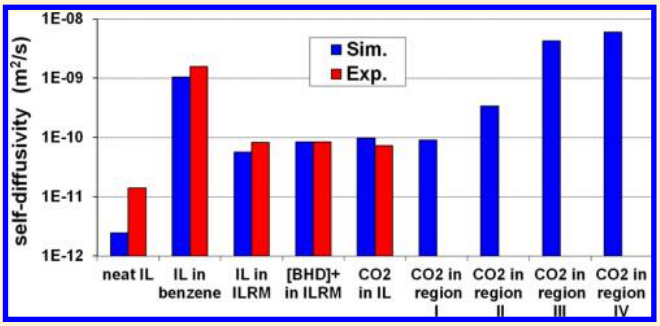

ABSTRACT: The structure and dynamics for CO_2 absorption in ionic liquid reverse micelle (ILRM) were studied using molecular simulations. The ILRM consisted of 1-butyl-3-methylimidazolium tetrafluoroborate ([bmim][BF_4]) ionic liquid (IL) as the micelle core, the benzylhexadecyldimethylammonium ([BHD]$^+$) chloride ([Cl]$^-$) was the cationic surfactant, and benzene was used as the continuous solvent phase in this study. The diffusivity values of this ILRM system were also experimentally determined. Simulations indicate that there is ion exchange between the IL anion ([BF_4]$^-$) and the surfactant anion ([Cl]$^-$). It was also found that the [bmim][BF_4] IL exhibits small local density at the interface region between the IL core and the [BHD]$^+$ surfactant cation layer, which leads to a smaller density for the [bmim][BF_4] IL inside the reverse micelle (RM) compared with the neat IL. These simulation findings are consistent with experimental results. Both our simulations and experimental results show that [bmim][BF_4] inside the RM diffuses 5−26 times faster than the neat IL, which is partly due to the fast *particle* diffusion for the ILRM nanodroplet (IL and surfactant) as a whole in benzene solvent compared with neat [bmim][BF_4] diffusion. Additionally, it was found that [bmim][BF_4] IL solved in benzene diffuses 2 orders of magnitude faster than the neat IL. Lastly, simulations show that CO_2 molecules are absorbed in four different regions of the ILRM system, that is, (I) in the IL inner core, (II) in the [BHD]$^+$ surfactant cation layer, (III) at the interface between the [BHD]$^+$ surfactant cation layer and benzene solvent, and (IV) in the benzene solvent. The CO_2 solubility was found to decrease in the order II > III ∼ IV > I, while the CO_2 diffusivity and permeability decrease in the following order: IV > III > II > I.

1. INTRODUCTION

Microemulsions are macroscopically homogeneous, thermodynamically stable dispersions of two immiscible liquids stabilized by a surfactant. Ionic liquid (IL) microemulsions, in which at least one of the components is an IL, have recently attracted much attention[1−4] due to their potentials as reaction and extraction media.[5,6] Many IL microemulsion systems, such as IL-in-oil,[7−10] oil-in-IL,[9,10] IL-in-water,[11] water-in-IL,[11] IL-in-CO_2,[12] CO_2-in-IL,[13] and IL-in-IL microemulsions,[14] have been studied.

Several groups have experimentally studied the IL-in-oil systems, in which the IL droplet is enclosed by surfactant molecules and stabilized in a continuous oil phase. This type of ionic liquid reverse micelle (RM) is generally denoted as IL/surfactant/oil. For the [P_{13}][Tf_2N]/Triton X-100/benzene ionic liquid reverse micelle (ILRM) system, Sarkar et al. have found that the diffusivity for the [P_{13}]$^+$ cation in the ILRM system is 1.74 times larger compared with the neat IL.[10] In the case of the [bmim][BF_4]/[BHDC]/benzene ILRM system, Falcone et al. have found that the [bmim][BF_4] IL inside the RM exhibits a smaller density than the corresponding neat IL.[15] It was also found that IL forms a layered structure in the RM.[15] Note that [bmim][BF_4] indicates the 1-butyl-3-methylimidazolium tetrafluoroborate IL and [BHDC] represents the benzylhexadecyldimethylammonium ([BHD]$^+$) chloride ([Cl]$^-$) cationic surfactant. The above experimental findings suggest that IL molecules confined in a RM will exhibit different structural arrangements and properties than the neat IL.

Despite the above experimental findings, the IL structures and properties in the ILRM system are yet to be understood. Several theoretical methods have been proposed to investigate RM systems. These methods include the molecular thermodynamics[16,17] method, the quantitative structure−property

Received: September 13, 2014
Revised: October 26, 2014

 © XXXX American Chemical Society

relationship approach,[18] the atomistic molecular dynamics (MD) simulations,[19−21] the Monte Carlo (MC) simulation using a lattice model,[22,23] and the dissipative particle dynamics simulations.[24,25] For the ILRM system, Chandran et al. have investigated the spontaneous ILRM formation using MD simulations for several IL/*N*-EtFOSA/CO_2 systems,[26] in which CO_2 acts as the continuous solvent phase and *N*-EtFOSA indicates the *N*-ethyl perfluorooctyl sulfonamide ($C_2H_5NHSO_2C_8F_{17}$) surfactant. It was found that the interactions between the anion of IL and the surfactant headgroup play a significant role in determining the ILRM stability.

Ionic liquids have been extensively studied[27−35] for gas separation applications due to their desired properties, such as negligible volatility, high thermal stability, nonflammability, and large CO_2 solubility. However, ILs have some drawbacks such as the high viscosity and large hygroscopicity.[36−38] In the case of high viscosity, slow mass transport of gases in ILs results in increased reactor size, and in the case of hygrophilicity, the large amount of absorbed water must be removed at substantial cost. Both factors substantially degrade the efficiency and economics of carbon capture.

Ionic liquid reverse micelle systems potentially can overcome the above two drawbacks. The small size and consequently the large specific area for the ILRM nanodroplet (IL and surfactant) will help gas mass transport. Additionally, a hydrophobic solvent is used as the continuous phase to minimize water permeation through the ILRM system, which may alleviate problems related to water absorption in ILs. Herein, we have studied the structure and dynamics of the [bmim][BF_4]/[BHDC]/benzene ILRM system both from experiment and molecular modeling. Finally, we have also studied CO_2 absorption into this ILRM system via molecular simulation.

2. SIMULATION DETAILS

2.1. Classical Force Field (FF). The molecular structures for the [bmim]$^+$ cation, [BF_4]$^-$ anion, [BHD]$^+$ surfactant cation, [Cl]$^-$ surfactant anion, and benzene solvent are shown in Figure 1. The classical FF potential used to simulate the

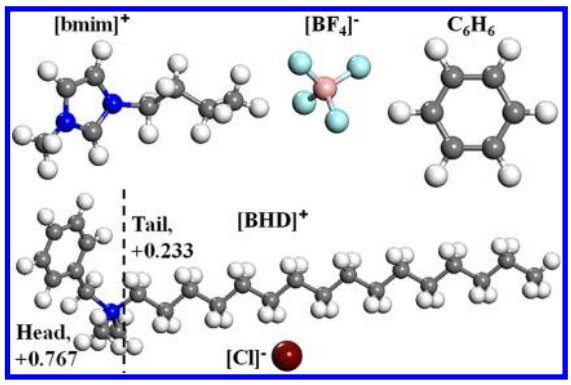

Figure 1. Molecular structures for 1-butyl-3-methylimidazolium cation ([bmim]$^+$), tetrafluoroborate anion ([BF_4]$^-$), benzylhexadecyldimethylammonium surfactant cation ([BHD]$^+$), chloride surfactant anion ([Cl]$^-$), and benzene (C_6H_6). A vertical dashed line was used to divide [BHD]$^+$ into two groups, that is, the headgroup with a charge of +0.767 e and the alkyl chain tail group with a charge of +0.233 e. Note that the charges were obtained from quantum *ab initio* calculations of [BHD]$^+$ in the gas phase.

[bmim][BF_4] IL, [BHDC] surfactant, benzene solvent, CO_2, and the interactions between these molecules is given by

$$\mathcal{V}(r) = \sum_{\text{bonds}} k_b(r - r_0)^2 + \sum_{\text{angles}} k_\theta(\theta - \theta_0)^2 + \sum_{\text{dihedrals}} k_\chi[1 + \cos(n_0\chi - \delta_0)] + \sum_{\text{impropers}} k_\psi(\psi - \psi_0)^2 + \sum_{i=1}^{N-1}\sum_{j=i+1}^{N}\left\{4\epsilon_{ij}\left[\left(\frac{\sigma_{ij}}{r_{ij}}\right)^{12} - \left(\frac{\sigma_{ij}}{r_{ij}}\right)^{6}\right] + \frac{q_i q_j}{r_{ij}}\right\} \quad (1)$$

where the symbols represent their conventional meanings.[39] Standard Lorentz−Berthelot combining rules were used to calculate the mixed Lennard-Jones (LJ) interaction parameters. The LJ potential was switched from 10.5 to 12.0 Å. A Verlet neighbor list with a 13.5 Å radius was used. The intramolecular electrostatic and LJ interactions for atoms separated by exactly three consecutive bonds were scaled by 0.5 and were neglected for atoms separated by less than three consecutive bonds.

The classical FF parameters for [bmim]$^+$, [BF_4]$^-$, and CO_2 were obtained from previous work[40−42] except that the σ values for the B and F atoms of the [BF_4]$^-$ anion[41] were decreased by 10% to give a simulated [bmim][BF_4] density to be more consistent with the experimental data. The LJ parameters for the [Cl]$^-$ surfactant anion were also obtained from previous work,[43] and they were set to be ϵ = 0.0355910 kcal/mol and σ = 4.4776570 Å. For the benzene solvent, both a united-atom model and an all-atom model were used. In the case of the united-atom benzene model, the FF parameters obtained by Siepmann et al.[44] were used except that the σ value for the CH united-atom group was decreased by 2.5% to give a simulated benzene density to be close to the experimental data. Note that a fixed united-atom benzene model was used by Siepmann, while a flexible united-atom model was used in this work. In the flexible model, the FF parameter values for $k_{b,CH-CH}$, $k_{\theta,CH-CH-CH}$, and CH−CH−CH−CH dihedral potential were taken from the CHARMM par_all36_cgenff.prm[45] file, in which the CG2R61 atom type was assigned to the CH united-atom group. In the case of the all-atom benzene model, all FF parameters were taken from the CHARMM par_all36_cgenff.prm[45] file except for $r_{0,C-C}$ = 1.394 Å and $r_{0,C-H}$ = 1.084 Å, which were obtained from *ab initio* gas phase optimization calculation at the B3LYP/6-311++g(d,p) level of theory. In this work, most of the simulation results were obtained by using the united-atom benzene model.

Solvent molar volume and/or density are one of the important factors to determine gas solubility, which will be calculated in this work. Consequently, the LJ σ values were tuned to match the experimental density for [bmim][BF_4] and benzene. In the case of [bmim][BF_4] ionic liquid, each [BF_4]$^-$ anion contains five atoms, which are less than 25 atoms contained in each [bmim]$^+$ cation. We chose to tune the LJ σ values for [BF_4]$^-$ anion rather than for [bmim]$^+$. In this way, we will have the least number of modifications for the classical force field parameters. Note that Maginn and co-workers have scaled the LJ σ values for atoms in cations to match the experimental IL density.[40] It would be interesting to compute the radial distributions and structures for [bmim][BF_4] using both the unaltered and modified LJ σ values for [BF_4]$^-$ and

compare them with the ab initio molecular dynamics simulations. However, these calculations are out of the scope of this work and hence they were not performed. In summary, only the σ values for B and F atoms of $[BF_4]^-$ anion and the σ value for the CH united atom of C_6H_6 were modified in this work. They were set to be σ_B = 3.2232716 Å, σ_F = 2.8063310 Å, and σ_{CH} = 3.6029993 Å.

For the $[BHD]^+$ surfactant cation, the r_0 and θ_0 values were obtained from *ab initio* gas phase optimization calculation. The charges were obtained from the CHELPG calculation. All *ab initio* calculations were performed at the B3LYP/6-311++g(d,p) level by using the Gaussian 09 program.[46] The k_b and k_θ force constants and the dihedral and LJ potential parameters were taken from the CHARMM par_all36_cgenff.prm file. All the FF parameters for the $[BHD]^+$ surfactant cation can be found in the Supporting Information.

2.2. Preparing Initial Configurations for the ILRM System. For the ILRM simulations, both random and predefined configurations were used as the starting configurations to investigate the effects of the initial configuration on the ILRM formation. For the random configuration, the $[bmim]^+$ cation, $[BF_4]^-$ anion, $[BHD]^+$ surfactant cation, $[Cl]^-$ surfactant anion, and benzene solvent molecules were randomly put in the simulation box. A representative random configuration is shown in Figure 2 (corresponding to t = 0 ns).

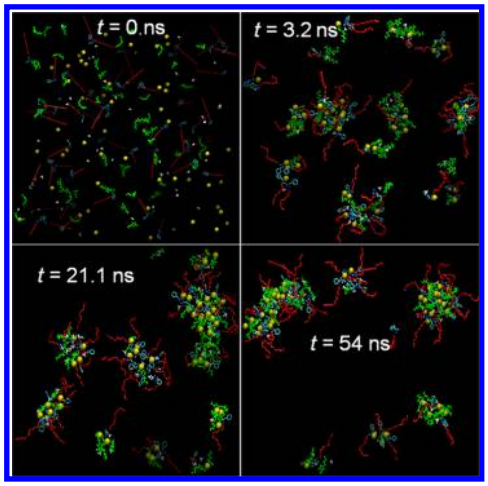

Figure 2. Representative snapshots obtained from NPT molecular dynamics simulations at 298 K and 1 bar. The system has 45290 atoms and contains 50 $[bmim][BF_4]$, 50 [BHDC], and 6690 benzene molecules. The simulation was started (t = 0 ns) from a random configuration. The symbols are as follows: green and white sticks for $[bmim]^+$ cation and $[BF_4]^-$ anion, respectively; cyan bond for the headgroup of $[BHD]^+$ surfactant cation; red bond for the alkyl chain tail of $[BHD]^+$ surfactant cation (Figure 1); and yellow sphere for the $[Cl]^-$ surfactant anion. Benzene solvent molecules are not shown for clarity.

The predefined configuration was obtained by using the following procedure, a similar method of which has also been used by Senapati et al.[47] to prepare the starting structure in the MD simulations for RM systems.

Step 1. A 10 ns NPT MD simulation was performed for the neat $[bmim][BF_4]$ IL at 298 K and 1 bar in cubic boxes, which contain 300−1100 ion pairs. The last snapshot was saved to prepare a spherical IL droplet using the following method:

1. For the above last snapshot, periodic boundary condition was used to put all the cations and anions in the image boxes back in the central box. The center of mass for the whole IL system was then shifted to the origin (the center of the simulation box). Ions were removed from the system if their centers of mass are far away from the origin with distances larger than a preset value of R. Several other cations or anions are also deleted to make the whole system be neutrally charged.
2. Using the above approach, a sphere with a radius of 16 Å was obtained which contains 50 $[bmim]^+$ and $[BF_4]^-$ ion pairs. Similarly, another two spherical droplets with radii of 20 and 31 Å were prepared, which consist of 100 and 400 ion pairs, respectively. These three IL droplets roughly have the neat IL density.

Step 2. Using locally developed software, 100−200 $[BHD]^+$ surfactant cations were evenly put on the outside spherical surface of the above three nanodroplets. The headgroup of the $[BHD]^+$ cation (Figure 1) was put on the spherical surface with the $[BHD]^+$ alkyl chain tail pointing outward. To avoid atom−atom overlaps (i.e., <2.0 Å), any newly added $[BHD]^+$ cation was discarded when the overlap occurred. Finally, 100−200 $[Cl]^-$ surfactant anions were randomly added in the systems.

Step 3. For the above ILRM nanodroplets obtained in step 2, 1000 steps of minimization and 1 ns NVT MD simulation were performed in the vacuum. These simulations were used to remove bad atom−atom contacts and obtain reasonable starting configurations for ILRM nanodroplets in the oil phase.

Step 4. The ILRM nanodroplet obtained in step 3 was put in an empty sphere, around which benzene molecules were added. The whole system was put in a cubic simulation box. A representative configuration for the ILRM nanodroplet immersed in the benzene solvent is shown in Figure 3a.

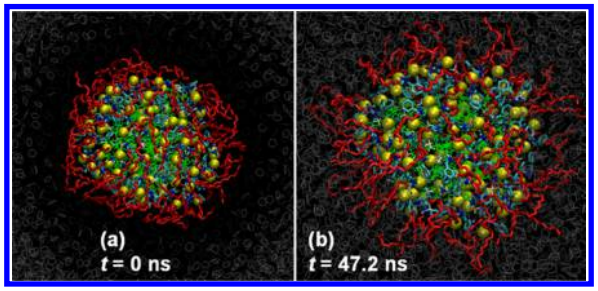

Figure 3. Representative snapshots obtained from NPT molecular dynamics simulations at 298 K and 1 bar. The ionic liquid reverse micelle (ILRM) system has 55798 atoms and contains 50 $[bmim][BF_4]$ IL, 100 [BHDC] surfactant, and 7833 benzene molecules. The simulation was started (corresponding to time t = 0 ns) from a predefined ILRM nanodroplet (IL and surfactant) structure. Benzene molecules are indicated by gray sticks. The other molecules are represented in the same way as in Figure 2.

Using the above procedure, three predefined ILRM structures in benzene were prepared. The ILRM 1 system contains 50 $[bmim][BF_4]$ IL, 100 [BHDC] surfactant, and 7833 C_6H_6 solvent molecules, which in total has 55798 atoms. The cubic simulation box length for the ILRM 1 system is about 108 Å. The ILRM 2 system consists of 80912 atoms and contains 100 IL, 200 [BHDC], and 10552 C_6H_6 molecules. The cubic box length for the ILRM 2 system is about 120 Å. The ILRM 3 system contains 95600 atoms and is composed of 400 IL, 200 [BHDC], and 11500 C_6H_6 solvent molecules. The

Table 1. Simulated (sim.) Densities (ρ) for Neat [bmim][BF_4], Neat [bmim][Cl], and Neat Benzene at 298−373 K and 1 bar[a]

	$\rho_{[bmim][BF_4]}$ (g/cm^3)		$\rho_{[bmim][Cl]}$ (g/cm^3)		$\rho_{C_6H_6}$ (g/cm^3)		
T (K)	sim.	exp.[55,56]	sim.	exp.[57,58]	sim. (united)	sim. (all)	exp.[59]
298	1.2145 (3)	1.21103	0.9563 (7)	1.0744	0.8661 (4)	0.8423 (3)	0.8736
303	-	-	-	-	0.8595 (1)	0.8356 (2)	0.8683
313	1.201 (1)	1.19044	0.947 (1)	1.0652	0.8474 (2)	0.8231 (3)	0.8577
373	1.1502 (4)	1.1469	0.9083 (6)	1.0426	-	-	-

[a]For benzene, both united-atom (united) and all-atom (all) benzene models were used to compute the density. The uncertainty in the last digit is given in parentheses. The experimental (exp.) densities are also shown for comparison. The "-" symbols indicate that the results are not available.

cubic box length for the ILRM 3 system is about 125 Å. Note that the united-atom benzene model was used in these three systems.

2.3. MD Simulation Details. For the neat benzene, [bmim][BF_4], and [bmim][Cl] ILs, 10 ns NPT simulation runs were performed at 298−373 K and 1 bar to compute the density. Following the NPT simulations, 10−20 ns NVE MD simulations were performed at 298−373 K to obtain the self-diffusivity values. Similarly, for the mixture consisting of five [bmim][BF_4] IL and 1000 benzene solvent molecules, NVE MD simulation was performed to compute the IL self-diffusivity in benzene.

When using a random initial configuration (Figure 2 at t = 0 ns) as the starting configuration in simulations for the ILRM system, a 50 ns NPT MD run was performed at 298 K and 1 bar to investigate the spontaneous ILRM nanodroplet formation in benzene. In the case of using predefined structures as starting configurations (Figure 3a), 30−170 ns NPT MD simulations were performed, following which 10−30 ns NVE MD simulations were carried out to obtain the self-diffusivities and the ILRM nanodroplet structures. All MD simulations were performed using the NAMD program.[48] The time step in MD simulations was set to be 0.5−1.0 fs. The particle-mesh Ewald method was used to compute the electrostatic interactions.

2.4. MC Simulation Details. To compute CO_2 solubilities in neat benzene, [BHDC], and [bmim][BF_4] systems, the continuous fractional component (CFC) MC method[42,49] was used. Simulations were performed at 298 K and CO_2 pressures of 4−17.15 bar. For the benzene system, 300 benzene molecules were used. In the case of neat [bmim][BF_4] IL, 160 ion pairs were used. For the neat [BHDC] system, 100 pairs of $[BHD]^+$ cations and $[Cl]^-$ anions were used. Simulation details for the CFC MC method can be found in the previous work.[42,50]

3. EXPERIMENTAL DETAILS

3.1. Preparation of ILRM. The [BHDC] surfactant was purchased from Sigma and was recrystallized twice by using the ethyl acetate. The [BHDC] powder was then dried at 50 °C overnight in a vacuum oven. An 18 g portion of [bmim][BF_4] (BASF quality, ≥98%, Sigma) was mixed with 20 mL of acetone and 6.5 g of active charcoal. The mixture was refluxed at 60 °C for 48 h. The active charcoal was removed by vacuum filtration, and the collected solution was further purified by using a 0.2 μm PTFE filter. Acetone was finally removed on a rotary evaporator under reduced pressure (100 Torr) at 45 °C. The purified [bmim][BF_4] IL was stored for further use. The deuterated benzene solvent (benzene-D_6, Sigma) was used as received.

The procedure to prepare the ILRM has been described elsewhere.[15] 0.3 M BHDC solution in benzene-D_6 was prepared first. The solution was filtrated through a 0.2 μm PTFE filter before use. In order to prepare an ILRM with a certain W value (W = moles of IL/molecules of surfactant), a given volume of [bmim][BF_4] was added to 0.5 mL BHDC solutions. Three clear ILRM solution samples with different W values (0.5, 1, and 1.5) were prepared.

Falcone et al.[15] have experimentally determined that these ILRM droplets exhibit diameters of 115−494 Å. On the basis of these diameter values, the volume of the solution, and the amounts of IL and surfactant, the ILRM nanodroplet−nanodroplet distance in our prepared samples was estimated to be larger than 50 Å. The experimental nanodroplet−nanodroplet distances are comparable to the simulated values of 35−50 Å (section 4.2.1), which suggests that the nanodroplet−nanodroplet interaction is minimized and the comparison between the simulation and experiment is meaningful.

3.2. NMR Diffusion Measurements. All the self-diffusion coefficient measurements were performed using a Bruker Avance III 600 MHz spectrometer with a BBFO probe with Z-axis gradient. Temperatures were controlled to ±1 K accuracy using a Bruker BVT3000 temperature control system. The samples were thermally equilibrated at a set temperature for 30 min before the measurement. All the experiments were performed with benzene-D_6 as the lock solvent. Extensive shimming was done on each sample prior to acquisition to observe JHH splitting. Measurements of the self-diffusion coefficients for the cation (ionic liquid cation and surfactant cation) and anion (ionic liquid anion) were performed by observing ^{1}H and ^{19}F, respectively. Self-diffusion coefficients were determined using a stimulated echo pulsed field gradient (STE-PFG) pulse sequence with bipolar gradients.[51,52] To obtain the self-diffusion coefficient, the peak intensity vs gradient strength data were fit to the Stejskal−Tanner equation[53,54]

$$I/I_0 = \exp[-\gamma^2 g^2 \delta^2 (\Delta - \delta/3) D]$$

where I and I_0 are the signal intensities with and without gradients, respectively, γ is the gyromagnetic ratio, g is the gradient strength, δ is the length of the gradient pulses, Δ is the diffusion time between the gradient pulses, and D is the self-diffusion coefficient. The gradient strength was varied between 0 and 50 G/cm, while the duration of the gradient δ was held constant throughout the experiment. δ was set between 2 and 5 ms, while the diffusion time Δ was kept constant at 100 ms depending on the diffusion rate of different samples.

4. RESULTS AND DISCUSSION

4.1. Thermodynamic and Dynamic Properties for [bmim][BF_4], [bmim][Cl], and C_6H_6. *4.1.1. Density for Neat [bmim][BF_4], [bmim][Cl], and C_6H_6.* To evaluate the

Table 2. Simulated (sim.) Self-Diffusivity Coefficients (D) for Neat [bmim][BF_4] and Neat Benzene at 1 bar[a]

	pure, 298 K	pure, 313 K	pure, 373 K	mix., 298 K
sim. $D_{[bmim]^+}$ (m^2/s)	$3.0(1) \times 10^{-12}$	$6.4(2) \times 10^{-12}$	$9.38(8) \times 10^{-11}$	$1.04(4) \times 10^{-9}$
sim. $\beta_{[bmim]^+}$	0.81(2)	0.77(1)	0.957(5)	0.96(3)
sim. $D_{[BF_4]^-}$ (m^2/s)	$1.9(1) \times 10^{-12}$	$4.6(1) \times 10^{-12}$	$6.6(1) \times 10^{-11}$	$1.05(4) \times 10^{-9}$
sim. $\beta_{[BF_4]^-}$	0.74(5)	0.80(2)	0.93(1)	0.96(4)
exp. $D_{[bmim]^+}$ (m^2/s)	1.47×10^{-11}	-	-	$\sim 10^{-9}$
exp. $D_{[BF_4]^-}$ (m^2/s)	1.37×10^{-11}	-	-	1.58×10^{-9}
sim. $D_{C_6H_6}$ (united) (m^2/s)	$4.08(1) \times 10^{-9}$	-	-	$4.08(1) \times 10^{-9}$
sim. $\beta_{C_6H_6}$ (united)	1.001(2)	-	-	1.001 (2)
sim. $D_{C_6H_6}$ (all) (m^2/s)	$2.163(4) \times 10^{-9}$	-	-	-
sim. $\beta_{C_6H_6}$ (all)	0.998(2)	-	-	-
exp. $D_{C_6H_6}$ (m^2/s)	2.27×10^{-9}	2.915×10^{-9}	-	-

[a]For neat benzene, both united-atom (united) and all-atom (all) benzene models were used to compute D. For [bmim][BF_4]−C_6H_6 mixture (mix.), the united-atom benzene model was used to compute the self-diffusivity coefficients. The $\beta = d(\log \Delta r^2)/d(\log t)$ values are also shown. Uncertainties in the last digit obtained from block average calculations are given in parentheses. For comparison, the experimental (exp.) D values for [bmim][BF_4] in neat ionic liquid and [bmim][BF_4]−C_6H_6 mixture obtained in this work and the experimental D data for neat C_6H_6 in the literature[60] are also shown. The "-" symbols indicate that the results are not available.

force field parameters for $[bmim]^+$, $[BF_4]^-$, $[Cl]^-$, and C_6H_6, the densities for neat [bmim][BF_4], [bmim][Cl], and C_6H_6 were calculated (Table 1) from the NPT MD simulations. The simulated [bmim][BF_4] densities at 298−373 K are very close to the experimental values,[55,56] with a difference smaller than 1%. The simulated [bmim][Cl] densities at 298−373 K are about 10% smaller than the experimental data.[57,58] For benzene, the united-atom and all-atom models give densities about 1.0 and 4.0% smaller than the experimental values,[59] respectively. Note that in this work the σ values for $[BF_4]^-$ anion and the united-atom C_6H_6 model were tuned to match the experimental data. Consequently, the difference between the simulated densities and the experimental data for [bmim][BF_4] IL and C_6H_6 are small. Even though the LJ parameters for $[Cl]^-$ were not tuned in this work, the simulated [bmim][Cl] densities are comparable to the experimental data, with an appreciable difference of about 10%. Note that the force field parameters for $[bmim]^+$ and $[Cl]^-$ used in this work were obtained from different groups;[40,43] they were developed not necessarily to reproduce the experimental density for [bmim][Cl] IL.

4.1.2. Self-Diffusivity for Neat [bmim][BF_4], C_6H_6, and Their Mixture. The simulated self-diffusion (D) coefficients for neat [bmim][BF_4] and benzene and the D values in their mixture are shown in Table 2. For neat benzene at 298 K, the all-atom benzene model gives self-diffusivity only 4.7% smaller than the experimental value.[60] In contrast, the united-atom benzene model predicts a self-diffusivity value about 80% larger than the experimental data. Note that both the all-atom and united-atom models give densities close to the experimental data. These findings suggest that self-diffusivity is more sensitive to the model than density. In this work, the united-atom benzene model was used to speed up simulations even though the all-atom benzene model gives a more accurate self-diffusivity value.

For neat [bmim][BF_4] IL at 298 K, the simulated D values for $[bmim]^+$ cation and $[BF_4]^-$ anion are 4.9−7.2 times smaller than the experimental data. This smaller simulated IL self-diffusivity is partly due to the nonpolarizable force field[61] for IL. Note that β values for the IL at 298 K are smaller than 1.0, which suggests that longer simulations are needed to get more accurate D values. Note that the experimental self-diffusivity value for $[bmim]^+$ is only slightly (7%) larger than that for $[BF_4]^-$ in the neat IL. In contrast, the simulated self-diffusivity for $[bmim]^+$ is significantly (58%) larger than that for $[BF_4]^-$. We have investigated whether the reduced σ values for $[BF_4]^-$ lead to this large difference. Using the unaltered σ values for $[BF_4]^-$, the self-diffusivity values for the neat IL were calculated to be $(4.8 \pm 0.1) \times 10^{-12}$ m^2/s for $[bmim]^+$ and $(2.6 \pm 0.1) \times 10^{-12}$ m^2/s for $[BF_4]^-$, respectively. The simulated self-diffusivity difference between $[bmim]^+$ and $[BF_4]^-$ becomes even larger (85%). Our other simulations (unpublished) for similar IL systems indicate that when the charges on the cations and anions were reduced from 1 to 0.8−0.9 e, which were obtained from ab initio molecular dynamics simulations, the self-diffusivity difference between cations and anions becomes smaller compared with the formal charge of 1 e. Hence, it is expected that using reduced charges for $[bmim]^+$ and $[BF_4]^-$ rather than 1 e (used in this work) could result in a smaller self-diffusivity difference between the cation and the anion.

For the mixture of [bmim][BF_4] solved in benzene, both simulations and experiments show that [bmim][BF_4] IL in the mixture exhibits 110−420 times larger self-diffusivity compared with the neat IL (Table 2 and Figure 11). Note that in simulation the mixture consists of five [bmim][BF_4] IL and 1000 benzene molecules. Simulations show that all five IL molecules aggregate to form a cluster in benzene after equilibration even though the cations and anions were initially put far away from each other at the start of the simulation. This IL cluster diffuses in the low viscous benzene solvent which leads to significantly enhanced IL self-diffusivity in benzene compared with the neat IL.

Note that the experimental data show both fast and slow IL diffusion coefficients in benzene. The fast diffusion coefficients are $\sim 10^{-9}$ m^2/s (Table 2), and the slow diffusion coefficients (not shown in Table 2) are 9.93×10^{-11} m^2/s for $[bmim]^+$ and 1.13×10^{-10} m^2/s for $[BF_4]^-$, respectively. For the experimental IL−benzene mixture, it is possible that both small and large IL clusters exist, which will lead to fast and slow IL diffusions, respectively. The slow IL diffusion coefficients in benzene are still 10 times larger compared with neat IL. Similarly, Sarraute et al. have experimentally determined that [bmim][BF_4], [bmim][Cl], and [hmim][Tf_2N] ILs also exhibit large self-diffusivity coefficients of $(0.58-3) \times 10^{-9}$ m^2/s in simple polar solvents such as water, methanol, and acetonitrile

at infinite dilution and 283−333 K.[62] Note that, although our simulations give the neat [bmim][BF_4] self-diffusivity to be 6 times smaller compared with the experimental data, the simulated and experimental IL self-diffusivities in the IL−benzene mixture are much closer to each other.

Finally, the self-diffusivity coefficients for neat [bmim][Cl] IL were also calculated at 298−373 K. Simulations indicate that [bmim][Cl] diffuses 2−3 times slower than [bmim][BF_4]. Additionally, the self-diffusivity coefficients for neat [BHDC] and [BHDC] in benzene were also calculated. Similar to the [bmim][BF_4]−benzene mixture, [BHDC] self-diffusivity in benzene is 2−3 orders of magnitude larger compared with the neat [BHDC]. Additionally, the five $[BHD]^+$−$[Cl]^-$ ion pairs also aggregate to form a large IL cluster in benzene.

4.2. Thermodynamic Properties for ILRM. *4.2.1. Starting Configuration Effect on ILRM Structure.* As shown in Figure 2 (t = 0), the [bmim][BF_4] IL, [BHDC] surfactant, and benzene solvent molecules were randomly placed in the simulation box at the start of the simulation, and later the RM-like structures form at t = 3.2, 21.1, and 54 ns. For the RM-like structure, the $[bmim]^+$ cations and $[BF_4]^-$ anions aggregate in the core to form an IL droplet, which is then enclosed by the $[BHD]^+$ surfactant cations. Some $[Cl]^-$ surfactant anions also occur in the IL droplet region, and other $[Cl]^-$ anions interact with the head of $[BHD]^+$. The alkyl chain tail of $[BHD]^+$ points outward and interacts with benzene solvent molecules. These findings indicate that the [bmim][BF_4] IL and [BHDC] surfactant molecules could spontaneously assemble into ILRM in benzene.

Starting from a predefined configuration, the ILRM structure in benzene remains at 47.2 ns (Figure 3) and at a much longer simulation time of 167 ns. At the start, the alkyl chains of $[BHD]^+$ surfactant cations lie on the RM outside surface. When the benzene molecules come closer to the ILRM, the alkyl chain tails of $[BHD]^+$ point outward to interact with benzene molecules. Note that, in all ILRM simulations, the micelle structure remains stable. If a big enough micelle was used as the predefined structure and long simulations were performed, the micelle may be divided into smaller ones.

Figures 2 and 3 indicate that the ILRM structure will spontaneously form in benzene. In the following analysis, the calculations are based on simulations starting from predefined configurations. Finally, it was found that the ILRM 1, ILRM 2, and ILRM 3 nanodroplets have radii of 30−45 Å. The closest distances between the ILRM nanodroplets in the central box and their images were estimated to be 35−50 Å, which would not result in significant interactions between them. The ILRM properties obtained for these three systems are not expected to be significantly different from the ILRM properties at low ILRM concentrations.

4.2.2. Local Density Profiles for ILRM. The local density distributions for each species in the ILRM 1 system are shown in Figure 4. Some $[BF_4]^-$ anions occur in the $[BHD]^+$ surfactant cation layer region probably due to the electrostatic interaction between the $[BF_4]^-$ anion and the headgroup of $[BHD]^+$ with a positive charge of 0.767 e (Figure 1). Some $[Cl]^-$ surfactant anions are absorbed in the [bmim][BF_4] IL droplet region to interact with the $[bmim]^+$ cation. Hence, ion exchange takes place between $[Cl]^-$ and $[BF_4]^-$, which is consistent with previous experiments.[15] Additionally, some benzene solvent molecules are absorbed in the $[BHD]^+$ surfactant cation layer region to interact with the alkyl chain tail of $[BHD]^+$ (Figure 3b). Several benzene molecules are also observed in the IL region possibly due to benzene interaction with the alkyl chain of the $[bmim]^+$ cation. The local density distributions for the ILRM 2 and ILRM 3 systems are similar to those for the ILRM 1 system.

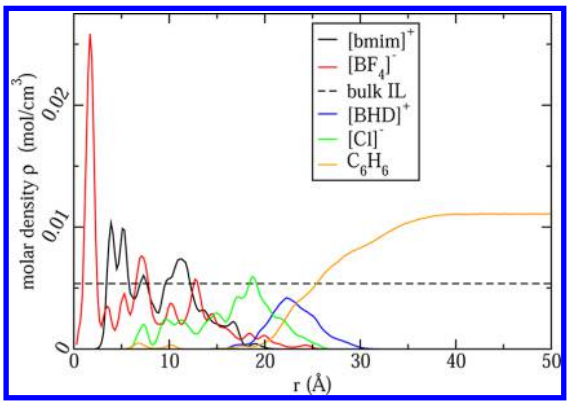

Figure 4. Local density distributions at 298 K for $[bmim]^+$ cation (solid black), $[BF_4]^-$ anion (solid red), $[BHD]^+$ surfactant cation (solid blue), $[Cl]^-$ surfactant anion (solid green), and C_6H_6 (solid orange) in the ionic liquid reverse micelle (ILRM) system. The origin was set to be the center of mass for all [bmim][BF_4] ionic liquid (IL) molecules. For comparison, the neat [bmim][BF_4] IL density at 298 K and 1 bar is also shown (horizontal dashed line). The ILRM system is the same as that in Figure 3b.

By doing the following integration

$$N = \int_{r_1}^{r_2} 4\pi r^2 \rho(r)\, \mathrm{d}r \tag{2}$$

where $\rho(r)$ is the local number density (Figure 4), the number of a species in the r range r_1−r_2 was calculated. At $0 \le r \le 16.1$ Å (Figure 4), the numbers were calculated to be 42.0 for $[bmim]^+$, 33.0 for $[BF_4]^-$, 20.4 for $[Cl]^-$, 0.1 for $[BHD]^+$, and 0.7 for C_6H_6. This range is mainly composed of IL molecules and $[Cl]^-$ surfactant anions, and it contains very few $[BHD]^+$ surfactant cations and C_6H_6 molecules. The total charge in this r range is −11 e, non-neutral. The [bmim][BF_4] mass density was calculated to be $(42 \times 139.22 + 33 \times 86.80)/(6.0221415 \times 4/3 \times \pi \times 16.1^3) = 0.828$ g/cm^3, about 32% less than 1.211 g/cm^3 for the neat [bmim][BF_4] IL at 298 K. The total mass density by including all species in this r range was calculated to be 0.906 g/cm^3, about 25% less than the neat IL density. For the ILRM 2 system, at $0 \le r \le 21.1$ Å, there are 92.0 $[bmim]^+$, 61.3 $[BF_4]^-$, and 58.0 $[Cl]^-$. Similar to the ILRM 1 system, the total charge in this r range is negative, about −27 e. The [bmim][BF_4] density in this region was calculated to be 0.765 g/cm^3, 60% less than the neat IL density. For the ILRM 3 system, at $0 \le r \le 29.1$ Å, there are 324.8 $[bmim]^+$, 224.3 $[BF_4]^-$, 117.4 $[Cl]^-$, and 4.7 C_6H_6. The [bmim][BF_4] density in this region was found to be 1.041 g/cm^3, still slightly smaller than the neat IL density. The total charge in this r range is −17 e.

For the [bmim][BF_4]/[BHDC]/benzene ILRM system, Falcone et al.[15] have experimentally determined that the [bmim][BF_4] IL density in RM is about 2 times smaller compared with neat IL, which is similar to our simulation findings. The smaller IL density in RM is partly due to the small local IL density in the interface region between the $[BHD]^+$ surfactant cation layer and the [bmim][BF_4] IL region, such as at 12 Å $\le r \le$ 16.1 Å (Figure 4).

4.3. Diffusivity of ILRM. *4.3.1. ILRM Particle Diffusion.* The ILRM nanodroplet particle, which consists of IL and surfactant molecules, diffuses as a whole in benzene solvent (Figure 5). The self-diffusivity coefficients for the ILRM 1, ILRM 2, and ILRM 3 nanodroplets at 298 K were calculated to be (3.8−5.3) × 10^{-11} m^2/s, which is larger than the experimental self-diffusivity values of (1.37−1.47) × 10^{-11} m^2/s for neat [bmim][BF_4]. The diffusion of the ILRM nanodroplet in benzene is denoted as *particle* diffusion in this work. The large ILRM *particle* diffusion coefficient is due to the low benzene viscosity. Compared with the diffusion of the smaller IL cluster (five [bmim][BF_4] ILs) in benzene, the much larger ILRM 1, ILRM 2, and ILRM 3 nanodroplets diffuse in benzene about 7−22 times slower (Figure 11). This is expected, since a larger particle diffuses slower than a smaller one.

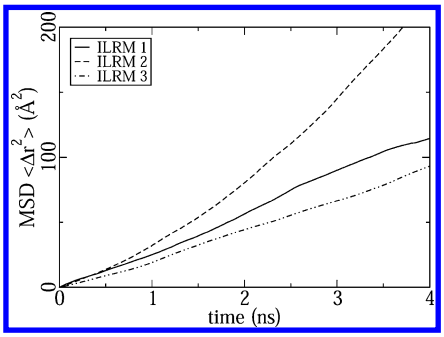

Figure 5. Mean squared displacement (MSD) for the center of mass of the ionic liquid reverse micelle (ILRM) nanodroplet at 298 K and 1 bar. Note that the center of mass was calculated by summing up all [bmim][BF_4] ionic liquid (IL) and [BHDC] surfactant molecules in the ILRM nanodroplet, which diffuses as a whole in benzene. The ILRM 1, 2, and 3 systems are the same as in Table 3.

4.3.2. Self-Diffusivity for IL and Surfactant Molecules in ILRM. Simulations suggest that $[bmim]^+$ and $[BF_4]^-$ in RM diffuse much faster than the neat [bmim][BF_4] IL (Figure 6). The self-diffusivity values for IL in RM are 16−35 times larger compared with neat IL (Tables 2 and 3 and Figure 11). Similarly, our experimental data indicate that the IL self-diffusivity in RM is 4−7 times larger compared with the neat IL. The significantly enhanced IL self-diffusivity in RM is partly due to the ILRM nanodroplet *particle* diffusion in benzene. The overall IL self-diffusivity in RM is composed of the IL diffusion along with the RM nanodroplet (*particle* diffusion) and the IL diffusion inside the RM nanodroplet (*intra* diffusion). Simulations indicate that the overall IL diffusion coefficients are 20−45% larger than the RM *particle* diffusion coefficients. Similarly, simulations suggest that the [BHDC] surfactant molecules in RM diffuse much faster than neat [BHDC] (not shown here). Furthermore, both our simulations and experiments show that the self-diffusivity coefficients for $[BHD]^+$ and [bmim][BF_4] IL in RM are comparable to each other (Table 3 and Figure 11), with a difference typically less than 35%. This result suggests that the diffusions for [bmim][BF_4] IL and $[BHD]^+$ surfactant cation are coupled as a result of ILRM nanodroplet *particle* diffusion. Note that all simulated self-diffusivity coefficients in Table 3 were obtained from 10 ns NVE MD simulations, which also agree with the diffusivities obtained from longer (20 ns) simulations.

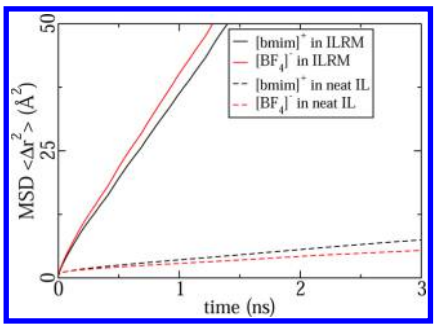

Figure 6. Mean squared displacement (MSD) for the $[bmim]^+$ cation (black line) and $[BF_4]^-$ anion (red line) at 298 K and 1 bar in the ionic liquid reverse micelle (ILRM) (solid line) and neat ionic liquid (IL) (dashed line) systems. The ILRM system consists of 50 [bmim][BF_4] IL, 100 [BHDC], and 7833 benzene molecules.

Although the simulated neat [bmim][BF_4] IL self-diffusivity is significantly (5.8 times) smaller (Table 2) than the experimental data, the simulated IL self-diffusivities in RMs are only 1.4 times smaller than the experimental values (Table 3 and Figure 11). Similarly, the simulated $[BHD]^+$ self-diffusivities in RMs are close to the experimental data. Note that the sizes of simulated ILRM nanodroplets are smaller than the experimental ones. If one assumes $D \propto 1/R$, where D is the IL self-diffusivity and R is the radius of the ILRM nanodroplet, from the experimental IL self-diffusivity values in RMs corresponding to $W = 1$ and $W = 1.5$ (Table 3), which have diameters of 115 and 258 Å,[15] respectively, the experimental IL self-diffusivity in the ILRM 3 system (diameter of 90 Å) is estimated to be 9.9 × 10^{-11} m^2/s, which is 1.8 times larger than the simulated value. This IL diffusivity difference in the ILRM system between the simulation and the experiment is not significantly large compared to the neat IL diffusivity difference between the simulation and the experiment.

The above simulated self-diffusivities for [bmim][BF_4] and [BHDC] in the ILRM systems were obtained by using a united-atom model for the benzene solvent. Although the all-atom benzene model gives 2 times smaller benzene self-diffusivity than the united-atom benzene model, it predicts self-diffusivities for [bmim][BF_4] and [BHDC] in the ILRM 1 system to be only 20% smaller compared with the IL and [BHDC] self-diffusivity coefficients by using the united-atom benzene model.

4.4. CO_2 Absorption into ILRM. *4.4.1. CO_2 Solubility. CO_2 Solubility in [bmim][BF_4], [BHDC], and C_6H_6.* Simulated CO_2 solubilities in neat [bmim][BF_4], [BHDC], and benzene are shown in Figure 7. The simulated CO_2 solubilities in [bmim][BF_4] are very close to the experimental data[63] below 10 bar. At a higher pressure of 17 bar, the simulated CO_2 solubility is still comparable to the experimental data, with a difference of 25%. The CO_2 solubilities in benzene and IL are close to each other. The CO_2 Henry's law constant in benzene at 298 K was estimated to be 88.90 bar by linear fitting of CO_2 solubilities at low CO_2 pressures. The CO_2 solubilities in [BHDC] are much larger than in [bmim][BF_4] and benzene, which is probably due to the long alkyl chain of $[BHD]^+$ cation leading to a large free volume for CO_2 absorption.

CO_2 Solubility in ILRM. As shown in Figures 8 and 9, CO_2 molecules are roughly absorbed at four different regions in the ILRM system, that is, the benzene solvent phase (region IV, $r \geq$ 40.1 Å), the interface region between the solvent and the $[BHD]^+$ surfactant cation layer (region III, 30.1 Å $\leq r \leq$ 40.1 Å), the $[BHD]^+$ surfactant cation layer (region II, 16.1 Å $\leq r \leq$

Table 3. Simulated (sim.) Self-Diffusivity Coefficients for $[bmim]^+$ Cation and $[BF_4]^-$ Anion in Different Ionic Liquid (IL) Reverse Micelle (RM) Systems at 298 K and 1 bar[a]

system	$[bmim]^+$	$[BF_4]^-$	$[BHD]^+$	$[Cl]^-$
sim. ILRM 1 (m^2/s)	$6.2(2) \times 10^{-11}$	$6.6(2) \times 10^{-11}$	$8.5(2) \times 10^{-11}$	$7.2(2) \times 10^{-11}$
sim. ILRM 2 (m^2/s)	$4.9(2) \times 10^{-11}$	$5.7(2) \times 10^{-11}$	$8.3(3) \times 10^{-11}$	$6.6(2) \times 10^{-11}$
sim. ILRM 3 (m^2/s)	$5.2(1) \times 10^{-11}$	$5.7(1) \times 10^{-11}$	$8.6(2) \times 10^{-11}$	$5.5(1) \times 10^{-11}$
exp. $W = 0.5$ (m^2/s)	8.11×10^{-11}	9.97×10^{-11}	9.31×10^{-11}	-
exp. $W = 1.0$ (m^2/s)	7.95×10^{-11}	9.75×10^{-11}	9.13×10^{-11}	-
exp. $W = 1.5$ (m^2/s)	6.10×10^{-11}	7.32×10^{-11}	6.89×10^{-11}	-

[a]The ILRM 1, 2, and 3 systems contain 50 IL/100 [BHDC]/7833 C_6H_6, 100 IL/200 [BHDC]/10552 C_6H_6, and 400 IL/200 [BHDC]/11500 C_6H_6, respectively. For comparison, the experimental (exp.) self-diffusivity values are also shown for three ILRM systems with different molar ratios (W) of $[bmim][BF_4]$ to [BHDC].

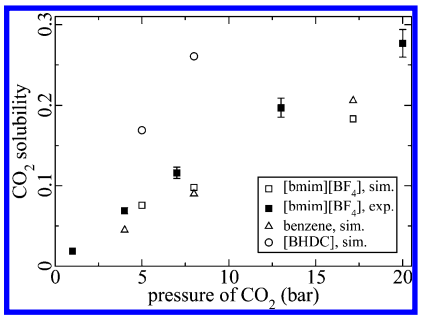

Figure 7. Simulated CO_2 solubilities (mole fraction) in neat $[bmim][BF_4]$ (open squares), neat benzene (triangles), and neat [BHDC] (circles) at 298 K. The experimental CO_2 solubilities in neat $[bmim][BF_4]$[63] (filled squares) are also shown for comparison. The simulation error bars are typically less than the size of the symbols, and only the experiment error bars are shown.

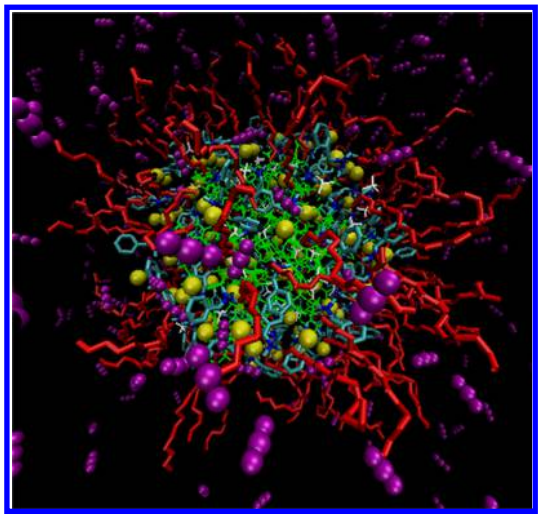

Figure 8. Representative snapshot for CO_2 absorption in an ionic liquid reverse micelle (ILRM) system at 298 K and 1 bar. The ILRM system contains 50 $[bmim][BF_4]$ IL, 100 [BHDC] surfactant, and 7833 benzene molecules, in which 500 CO_2 molecules are absorbed. The CO_2 molecules are indicated as purple VDW. The IL and surfactant molecules are represented in the same way as in Figure 2. Benzene solvent molecules are not shown for clarity.

30.1 Å), and the $[bmim][BF_4]$ IL region (region I, $0 \leq r \leq 16.1$ Å).

By performing integrations using eq 2, the numbers for each species in four regions of the ILRM system were calculated. In region I, calculations show that there are 1.5 CO_2 molecules, 41.6 $[bmim]^+$ cations, 32.5 $[BF_4]^-$ anions, 20.3 $[Cl]^-$ surfactant

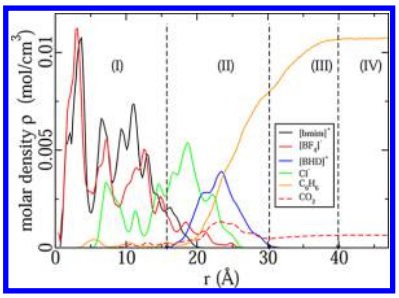

Figure 9. Local density distributions for CO_2 (dashed red) absorption in different regions of an ionic liquid reverse micelle (ILRM) system at 298 K and 1 bar. The CO_2–ILRM system is the same as in Figure 8. The origin was set to be the center of mass for all $[bmim][BF_4]$ ionic liquid (IL) molecules. Three vertical dashed lines are used to indicate four different regions of the ILRM system, that is, region I (IL region), region II ($[BHD]^+$ surfactant cation layer), region III (the interface region between region II and the benzene solvent phase), and region IV (the benzene solvent phase).

anions, and 1.4 benzene solvents. In region II, there are 45.2 CO_2, 8.4 $[bmim]^+$, 17.5 $[BF_4]^-$, 79.7 $[Cl]^-$, 99.4 $[BHD]^+$ surfactant cations, and 250 benzene molecules. Region III contains 55.2 CO_2, 0.6 $[BHD]^+$, and 926.1 benzene molecules. Region IV only consists of CO_2 and benzene molecules. The CO_2 mole fraction in region IV was calculated to be 0.057, which roughly corresponds to a CO_2 gas pressure of 5 bar (Figure 7).

In region I, the CO_2 molar fraction was calculated to be $x_{CO_2} = 1.5/(1.5 + 41.6 + 32.5 + 20.3 + 1.4) = 0.015$, which corresponds to a CO_2 Henry's law constant of $5/0.015 = 333.33$ bar. Similarly, the CO_2 Henry's law constants in regions II and III were calculated to be 55.31 and 89.29 bar, respectively. Note that the larger the Henry's law constant, the smaller the gas solubility. CO_2 solubilities at different regions of the ILRM 1 system decrease in the following order: region II > region IV ~ region III > region I (Table 4). CO_2 exhibits the largest gas solubility in the $[BHD]^+$ surfactant layer (region II). This is partly due to the long alkyl tail of the $[BHD]^+$ surfactant cation, which leads to loose packing between the tails and consequently a large free volume is available for CO_2 absorption (Figure 8). This result is also consistent with the finding that neat [BHDC] exhibits a larger CO_2 solubility than neat $[bmim][BF_4]$ and neat C_6H_6 (Figure 7). Interestingly, CO_2 solubility in the IL region I is about 2 times $(333.33/(88.90 \times 2) = 1.9)$ smaller than that in the neat $[bmim][BF_4]$. This is partly due to the presence of significant amounts of $[Cl]^-$ surfactant anions in region I. It has been experimentally determined that CO_2 exhibits a smaller

Table 4. Simulated CO_2 Henry's Law Constant (H), CO_2 Self-Diffusivity (D), and CO_2 Permeability (perm.) in Four Different Regions (Figure 9) of the Ionic Liquid Reverse Micelle (ILRM) System at 298 K[a]

		self-diffusivity		
region	H (bar)	D (m^2/s)	β	perm. (barrer)
I	333.33	$9.1(5) \times 10^{-11}$	1.05(6)	76 ± 4
II	55.31	$3.4(1) \times 10^{-10}$	0.92(3)	1433 ± 42
III	89.29	$4.31(6) \times 10^{-9}$	0.91(2)	14300 ± 200
IV	88.90	$5.98(4) \times 10^{-9}$	0.97(1)	22270 ± 150

[a]The ILRM system contains 50 [bmim][BF_4]/100 [BHDC]/7833 C_6H_6. A total number of 500 CO_2 molecules are absorbed in the ILRM system. Note that the summation of cation and anion numbers rather than the number of IL pairs was used to compute the CO_2 molar fraction and Henry's law constant. The $\beta = d(\log \Delta r^2)/d(\log t)$ values obtained from simulations are also shown. The uncertainty in the last digit is given in parentheses.

solubility in [bmim][Cl] IL than in [bmim][BF_4].[64,65] The $[Cl]^-$ anions in region I have taken up some free volumes which would otherwise contribute to CO_2 absorption.

4.4.2. CO_2 Diffusivity. Calculations of CO_2 self-diffusivity in four different regions of the ILRM system are complicated because a CO_2 molecule is not necessarily absorbed only in one region during the simulation. The CO_2 molecule may diffuse back and forth between different regions. Such an example is shown in Figure 10. From 0.35 to 5.35 ns, the CO_2 molecule is absorbed in region I. At 5.35 ns, it starts to diffuse into other regions. For example, the CO_2 molecule is absorbed in region IV at t = 8 ns. From 0.35 to 5.35 ns corresponding to region I, the CO_2 mean square displacement (MSD) was calculated. Similarly, another three CO_2 molecules were found to be absorbed in region I and their MSD values at the corresponding periods of time were also calculated. The CO_2 self-diffusivity in region I was then computed to be $(9.1 \pm 0.5) \times 10^{-11}$ m^2/s from the average of those four sets of MSD values. CO_2 self-diffusivity coefficients in regions II, III, and IV were also calculated (Table 4), which decrease in the following order: region IV > region III > region II > region I. Similar to [bmim][BF_4] diffusion in the RM, CO_2 diffusions in regions I and II consist of CO_2 *particle* diffusion along with the RM nanodroplet and CO_2 *intra* diffusion inside the RM. The overall CO_2 self-diffusivity coefficients in regions I and II are 1.7−6.4 times larger than the *particle* diffusion coefficient for the corresponding ILRM 1 nanodroplet. The larger CO_2 diffusivity in region II than in region I is partly due to the $[BHD]^+$ surfactant cation layer. The large free volume between the alkyl chain tails of the $[BHD]^+$ surfactant cations in region II may lead to a large CO_2 *intra* diffusivity. Region IV corresponds to the less viscous benzene solvent phase, and as a result, CO_2 exhibits the largest diffusivity in this region. Note that the β values for CO_2 diffusion in the ILRM system are very close to 1 (Table 4), which suggests that simulations are long enough to obtain reliable CO_2 self-diffusivities.

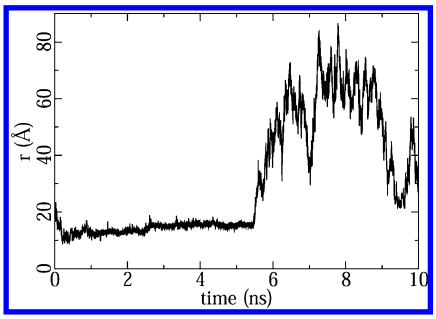

Figure 10. Center of mass for a CO_2 molecule absorbed in different regions of the ionic liquid reverse micelle (ILRM) system at 298 K and 1 bar. The CO_2−ILRM system is the same as that in Figure 8. The origin was set to be the center of mass for all [bmim][BF_4] ionic liquid molecules.

CO_2 self-diffusivity coefficients in neat [bmim][BF_4] and neat [BHDC] were also calculated. The CO_2 self-diffusivity in [bmim][BF_4] at 298 K was calculated to be $(9.9 \pm 0.1) \times 10^{-11}$ m^2/s (Figure 11), reasonably close to the experimental value of 7.3×10^{-11} m^2/s obtained by Shiflett et al.[63] Compared with neat [bmim][BF_4] and region I (mainly composed of [bmim][BF_4] IL) of the ILRM 1 system, CO_2 self-diffusivities in them were found to be close to each other. In neat [BHDC], CO_2 self-diffusivity was calculated to be $(4.0 \pm 0.1) \times 10^{-11}$ m^2/s, which is 8.5 times smaller than the CO_2 diffusivity in region II (mainly composed of [BHDC]) of the ILRM 1 system.

4.4.3. CO_2 Permeability in ILRM. CO_2 permeability in each region of the ILRM system was calculated by using $Pe = D/VH$, where Pe, D, and H are the CO_2 permeability, diffusivity, and Henry's law constant, respectively. V is the molar volume for the corresponding region of the ILRM system. To be consistent with the above CO_2 mole fraction calculation in the ILRM system and the subsequent CO_2 Henry's law constant computation, V was calculated by using the summation of cation and anion numbers rather than the number of IL pairs. For example, in region I, V was calculated to be $V = (4/3 \times \pi \times 16.1^3 \times 0.1 \times 6.0221415)/(1.5 + 41.6 + 32.5 + 20.3 + 1.4) = 108.2$ cm^3/mol. Consequently, CO_2 permeability in region I was calculated to be 76 ± 4 barrer. Similarly, CO_2 permeabilities in regions II, III, and IV were also calculated (Table 4) and they decrease in the following order at different regions: region IV > region III > region II > region I. Among all four regions of the ILRM system, region I gives both the smallest CO_2 solubility and the smallest CO_2 diffusivity (Table 4), which leads to the smallest CO_2 permeability in region I. CO_2 exhibits the largest permeability in region IV mainly due to its largest diffusivity (Table 4). Lastly, CO_2 permeability in neat [bmim][BF_4] was calculated to be 179 barrer, which is 2.4 times larger than CO_2 permeability in the IL region, i.e., region I of the ILRM 1 system. This result is partly due to the smaller CO_2 solubility in region I of the ILRM system compared with neat [bmim][BF_4].

5. CONCLUSIONS

In this work, the structure and dynamics for the [bmim][BF_4]−benzene mixture, the [BHDC]−benzene mixture, and the [bmim][BF_4]/[BHDC]/benzene ILRM system were studied using both molecular simulations and experiments. Simulations show that the ILRM is formed by spontaneous self-assembly of the [bmim][BF_4] IL and [BHDC] surfactant molecules in benzene. In the ILRM, some $[Cl]^-$ surfactant anions exchange with the $[BF_4]^-$ anions, and those $[Cl]^-$ surfactant anions are absorbed in the [bmim][BF_4] phase, the ILRM inner core region. Additionally, the [bmim][BF_4] IL density inside the RM was found to be smaller than the neat IL. All of these simulation results agree with previous experimental data.[15]

With regard to diffusivities for the [bmim][BF_4]−benzene and [BHDC]−benzene mixtures, both our simulations and

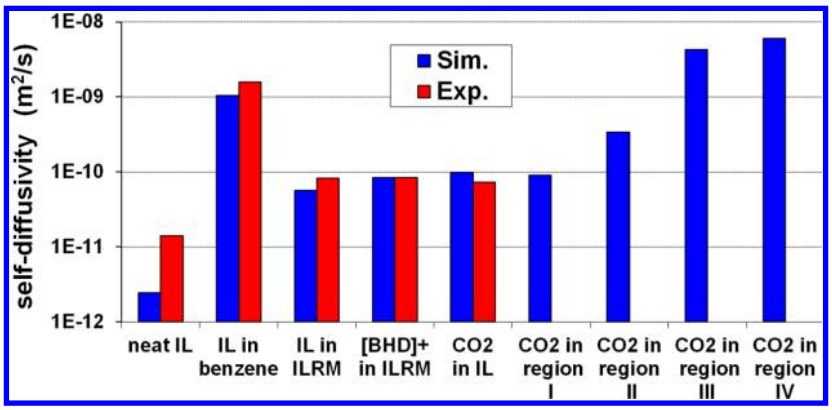

Figure 11. Summary of simulated (Sim.) and experimental (Exp.) self-diffusivity coefficients (D) for different systems at 298 K and 1 bar. For comparison, the [bmim][BF_4] self-diffusivities in neat ionic liquid (IL), the [bmim][BF_4]−benzene mixture, and the ionic liquid reverse micelle (ILRM) system are shown. The self-diffusivity for [bmim][BF_4] was calculated to be the average D values for $[bmim]^+$ cation and $[BF_4]^-$ anion. In the case of ILRM, the simulated and experimental self-diffusivity coefficients for [bmim][BF_4] and $[BHD]^+$ were calculated to be the corresponding average D values of three ILRM systems (Table 3). CO_2 self-diffusivity coefficients in neat [bmim][BF_4] and four different regions of the ILRM 1 system (Table 4) are also shown. For comparison, the experimental CO_2 diffusivity in neat IL obtained by Shiflett et al.[63] is also shown.

experiments show that when the [bmim][BF_4] IL is solved in benzene its self-diffusivity becomes 110−420 times larger compared with neat IL. The $[bmim]^+$ cations and $[BF_4]^-$ anions aggregate to form a large IL cluster in benzene even though the cations and anions were put far away from each other at the beginning of the simulations. Similarly, simulations show that the self-diffusivity for [BHDC] in benzene is 2−3 orders of magnitude larger compared with neat [BHDC].

For the ILRM nanodroplet, which consists of [bmim][BF_4] IL and the [BHDC] surfactant molecules, simulations show that it diffuses as a whole in the benzene solvent. The corresponding *particle* diffusion coefficients for three ILRM nanodroplets (radius of 30−45 Å) at 298 K were calculated to be $(3.8-5.3) \times 10^{-11}$ m^2/s, which are 3−20 times larger than the self-diffusivity for neat [bmim][BF_4]. The overall IL diffusivity in the ILRM nanodroplet consists of two parts, that is, the *particle* diffusion of IL along with the nanodroplet as a whole and the *intra* diffusion of IL inside the nanodroplet. Partly due to the *particle* diffusion, both our simulations and experiments show that the [bmim][BF_4] IL molecules in the ILRM nanodroplets diffuse 6−20 times faster than neat IL. Additionally, although simulations show that neat [BHDC] diffuses significantly slower than neat [bmim][BF_4], both simulations and experiments show that the self-diffusivity coefficients for [BHDC] surfactant and [bmim][BF_4] IL molecules in the ILRM systems are comparable to each other as a result of the ILRM nanodroplet *particle* diffusion.

As a final comparison between simulations and experiments, the simulated self-diffusivity for neat [bmim][BF_4] was found to be significantly (6 times) smaller than the experimental data, which is probably due to the neglect of IL polarizability in the classical force field. In contrast, the simulated [bmim][BF_4] self-diffusivity coefficients in benzene solvent and in ILRM systems were found to be close to the experimental data, with a small difference of only 10−40%. Similarly, the simulated self-diffusivities for $[BHD]^+$ surfactant cations in the ILRM systems are also close to the experimental data. Note that the simulated ILRM nanodroplets (radius of 30−45 Å) are typically smaller than the experimental ones (radius of 57.5 and 129 Å for $W = 1$ and $W = 1.5$, respectively). A more fair IL diffusivity comparison between simulation and experiment could be obtained by using the ILRM nanodroplets of the same size. Hence, the experimental IL self-diffusivity in the ILRM nanodroplet (radius of 45 Å) was estimated by extrapolating the experimental diffusivities, and found to be 9.9×10^{-11} m^2/s, which is only 80% larger than the simulated value corresponding to the ILRM 3 nanodroplet (radius of 45 Å).

Lastly, CO_2 solubility and diffusivity in the ILRM system were studied from molecular simulations. CO_2 molecules are absorbed into four regions of the ILRM system, that is, region I (mainly consisting of [bmim][BF_4] IL molecules), region II (the $[BHD]^+$ surfactant cation layer region), region III (the interface region between region II and the benzene solvent), and region IV (the benzene solvent region). CO_2 solubilities in these regions decrease in the following order: region II > region IV ∼ region III > region I. The largest CO_2 solubility in region II is partly due to the large free volume between the alkyl chain tails of the $[BHD]^+$ surfactant cations. Compared with neat [bmim][BF_4], CO_2 exhibits a smaller solubility in the IL region (region I) of the ILRM system. This is partly due to the presence of $[Cl]^-$ surfactant anions in region I, which compete for CO_2 absorption and decrease CO_2 solubility.

CO_2 diffusivity in four regions of the ILRM system decreases in the following order: region IV > region III > region II > region I. CO_2 exhibits the largest diffusivity in the less viscous benzene solvent phase. CO_2 diffusivity in region II is larger than that in region I, which is also partly due to the large free volume in the $[BHD]^+$ surfactant cation layer region. Although CO_2 solubility in region I (IL region) is smaller than that in neat IL, CO_2 diffusivities in region I and neat IL were found to be close to each other. CO_2 permeabilities were also calculated, and they decrease in the following order: region IV > region III > region II > region I. Among all four regions, CO_2 exhibits the smallest diffusivity and solubility, and consequently the smallest permeability in region I.

Note that this specific [bmim][BF_4]/BHDC/benzene ILRM system is not intended to be used for CO_2 capture, for [bmim][BF_4] IL has small CO_2 solubility and the benzene solvent is volatile. Other ILs, which have higher CO_2 solubility, and other nonvolatile solvents with low viscosity, will be investigated to form ILRMs for CO_2 capture.

■ ASSOCIATED CONTENT

Ⓢ Supporting Information

The force field parameters for $[BHD]^+$ surfactant cation. This material is available free of charge via the Internet at http://pubs.acs.org.

■ AUTHOR INFORMATION

Corresponding Author

*E-mail: shiw@netl.doe.gov.

Notes

The authors declare no competing financial interest.

■ ACKNOWLEDGMENTS

This project was funded by the Department of Energy, National Energy Technology Laboratory, an agency of the United States Government, through a support contract with URS Energy & Construction, Inc. Neither the United States Government nor any agency thereof, nor any of their employees, nor URS Energy & Construction, Inc., nor any of their employees, makes any warranty, expressed or implied, or assumes any legal liability or responsibility for the accuracy, completeness, or usefulness of any information, apparatus, product, or process disclosed, or represents that its use would not infringe privately owned rights. Reference herein to any specific commercial product, process, or service by trade name, trademark, manufacturer, or otherwise, does not necessarily constitute or imply its endorsement, recommendation, or favoring by the United States Government or any agency thereof. The views and opinions of authors expressed herein do not necessarily state or reflect those of the United States Government or any agency thereof.

■ REFERENCES

(1) Qiu, Z.; Texter, J. Ionic Liquids in Microemulsions. *Curr. Opin. Colloid Interface Sci.* **2008**, *13*, 252−262.

(2) Kunz, W.; Zemb, T.; Harrar, A. Using Ionic Liquids to Formulate Microemulsions: Current State of Affairs. *Curr. Opin. Colloid Interface Sci.* **2012**, *17*, 205−211.

(3) Greaves, T. L.; Drummond, C. J. Solvent Nanostructure, the Solvophobic Effect and Amphiphile Self-Assembly in Ionic Liquids. *Chem. Soc. Rev.* **2013**, *42*, 1096−1120.

(4) Shang, W.; Kang, X.; Ning, H.; Zhang, J.; Zhang, X.; Wu, Z.; Mo, G.; Xing, X.; Han, B. Shape and Size Controlled Synthesis of MOF Nanocrystals with the Assistance of Ionic Liquid Mircoemulsions. *Langmuir* **2013**, *29*, 13168−13174.

(5) Holmberg, K. Organic and Bioorganic Reacions in Microemulsions. *Adv. Colloid Interface Sci.* **1994**, *51*, 137−174.

(6) Dwars, T.; Paetzold, E.; Oehme, G. Reactions in Micellar Systems. *Angew. Chem., Int. Ed.* **2005**, *44*, 7174−7199.

(7) Gao, H.; Li, J.; Han, B.; Chen, W.; Zhang, J.; Zhang, R.; Yan, D. Microemulsions with Ionic Liquid Polar Domains. *Phys. Chem. Chem. Phys.* **2004**, *6*, 2914−2916.

(8) Eastoe, J.; Gold, S.; Rogers, S.; Paul, A.; Welton, T.; Heenan, R.; Grillo, I. Ionic Liquid-in-Oil Microemulsions. *J. Am. Chem. Soc.* **2005**, *127*, 7302−7303.

(9) Li, N.; Gao, Y.; Zheng, L.; Zhang, J.; Yu, L.; Li, X. Studies on the Micropolarities of bmimBF(4)/TX-100/toluene Ionic Liquid Microemulsions and Their Behaviors Characterized by UV-Visible Spectroscopy. *Langmuir* **2007**, *23*, 1091−1097.

(10) Pramanik, R.; Sarkar, S.; Ghatak, C.; Rao, V. G.; Sarkar, N. Ionic Liquid Containing Microemulsions: Probe by Conductance, Dynamic Light Scattering, Diffusion-Ordered Spectroscopy NMR Measurements, and Study of Solvent Relaxation Dynamics. *J. Phys. Chem. B* **2011**, *115*, 2322−2330.

(11) Gao, Y.; Han, S.; Han, B.; Li, G.; Shen, D.; Li, Z.; Du, J.; Hou, W.; Zhang, G. TX-100/water/1-butyl-3-methylimidazolium Hexafluorophosphate Microemulsions. *Langmuir* **2005**, *21*, 5681−5684.

(12) Liu, J.; Cheng, S.; Zhang, J.; Feng, X.; Fu, X.; Han, B. Reverse Micelles in Carbon Dioxide with Ionic-Liquid Domains. *Angew. Chem., Int. Ed.* **2007**, *46*, 3313−3315.

(13) Zhang, J.; Han, B.; Li, J.; Zhao, Y.; Yang, G. Carbon Dioxide in Ionic Liquid Microemulsions. *Angew. Chem., Int. Ed.* **2011**, *50*, 9911−9915.

(14) Cheng, S.; Zhang, J.; Zhang, Z.; Han, B. Novel Microemulsions: Ionic Liquid-in-Ionic Liquid. *Chem. Commun.* **2007**, 2497−2499.

(15) Falcone, R. D.; Baruah, B.; Gaidamauskas, E.; Rithner, C. D.; Correa, N. M.; Silber, J. J.; Crans, D. C.; Levinger, N. E. Layered Structure of Room-Temperature Ionic Liquids in Microemulsions by Multinuclear NMR Spectroscopic Studies. *Chem.—Eur. J.* **2011**, *17*, 6837−6846.

(16) Nagarajan, R.; Ruckenstein, E. Aggregation of Amphiphiles as Micelles or Vesicles in Aqueous-Media. *J. Colloid Interface Sci.* **1979**, *71*, 580−604.

(17) Puvvada, S.; Blankschtein, D. Molecular-Thermodynamic Approach to Predict Micellization, Phase-Behavior and Phase-Separation of Micellar Solutions. 1. Application to Nonionic Surfactants. *J. Chem. Phys.* **1990**, *92*, 3710−3724.

(18) Huibers, P.; Lobanov, V.; Katritzky, A.; Shah, D.; Karelson, M. Prediction of Critical Micelle Concentration Using a Quantitative Structure-Property Relationship Approach 0.2. Anionic Surfactants. *J. Colloid Interface Sci.* **1997**, *187*, 113−120.

(19) Abel, S.; Sterpone, F.; Bandyopadhyay, S.; Marchi, M. Molecular Modeling and Simulations of AOT-Water Reverse Micelles in Isooctane: Structural and Dynamic Properties. *J. Phys. Chem. B* **2004**, *108*, 19458−19466.

(20) Abel, S.; Waks, M.; Urbach, W.; Marchi, M. Structure, Stability, and Hydration of a Polypeptide in AOT Reverse Micelles. *J. Am. Chem. Soc.* **2006**, *128*, 382−383.

(21) Gardner, A.; Vasque, V. R.; Clifton, A.; Graeve, O. A. Molecular Dynamics Analysis of the AOT/Water/Isooctane System: Effect of Simulation time, Initial Configuration, and Model Salts. *Fluid Phase Equilib.* **2007**, *262*, 264−270.

(22) Mackie, A.; Onur, K.; Panagiotopoulos, A. Phase Equilibria of a Lattice Model for an Oil-Water-Amphiphile Mixture. *J. Chem. Phys.* **1996**, *104*, 3718−3725.

(23) Rodriguez-Guadarrama, L.; Ramanathana, S.; Mohanty, K.; Vasquez, V. Molecular Modeling of Binary Mixtures of Amphiphiles in a Lattice Solution. *Fluid Phase Equilib.* **2004**, *226*, 27−36.

(24) Ryjkina, E.; Kuhn, H.; Rehage, H.; Muller, F.; Peggau, J. Molecular Dynamic Computer Simulations of Phase Behavior of Nonionic Surfactants. *Angew. Chem., Int. Ed.* **2002**, *41*, 983−986.

(25) Yang, C.; Chen, X.; Qiu, H.; Zhuang, W.; Chai, Y.; Hao, J. Dissipative Particle Dynamics Simulation of Phase Behavior of Aerosol OT/Water System. *J. Phys. Chem. B* **2006**, *110*, 21735−21740.

(26) Chandran, A.; Prakash, K.; Senapati, S. Self-Assembled Inverted Micelles Stabilize Ionic Liquid Domains in Supercritical CO_2. *J. Am. Chem. Soc.* **2010**, *132*, 12511−12516.

(27) Brennecke, J. F.; Maginn, E. J. Ionic liquids: Innovative Fluids for Chemical Processing. *AIChE J.* **2001**, *47*, 2384−2389.

(28) Ramdin, M.; de Loos, T. W.; Vlugt, T. J. H. State-of-the-Art of CO_2 Capture with Ionic Liquids. *Ind. Eng. Chem. Res.* **2012**, *51*, 8149−8177.

(29) Anthony, J. L.; Aki, S. N. V. K.; Maginn, E. J.; Brennecke, J. F. Feasibility of Using Ionic Liquids for Carbon Dioxide Capture. *Int. J. Environ. Technol. Manage.* **2004**, *4*, 105−115.

(30) Yokozeki, A.; Shiflett, M. B.; Junk, C. P.; Grieco, L. M.; Foo, T. Physical and Chemical Absorptions of Carbon Dioxide in Room-Temperature Ionic Liquids. *J. Phys. Chem. B* **2008**, *112*, 16654−16663.

(31) Bates, E. D.; Mayton, R. D.; Ntai, I.; Davis, J. H. CO_2 Capture by a Task-Specific Ionic Liquid. *J. Am. Chem. Soc.* **2002**, *124*, 926−927.

(32) Gurkan, B.; Goodrich, B. F.; Mindrup, E. M.; Ficke, L. E.; Massel, M.; Seo, S.; Senftle, T. P.; Wu, H.; Glaser, M. F.; Shah, J. K.; et al. Molecular Design of High Capacity, Low Viscosity, Chemically

Tunable Ionic Liquids for CO_2 Capture. *J. Phys. Chem. Lett.* **2010**, *1*, 3494−3499.
(33) Myers, C.; Pennline, H.; Luebke, D.; Ilconich, J.; Dixon, J. K.; Maginn, E. J.; Brennecke, J. F. High Temperature Separation of Carbon Dioxide/Hydrogen Mixtures Using Facilitated Supported Ionic Liquid Membranes. *J. Membr. Sci.* **2008**, *322*, 28−31.
(34) Shi, W.; Myers, C. R.; Luebke, D. R.; Steckel, J. A.; Sorescu, D. C. Theoretical and Experimental Studies of CO_2 and H_2 Separation Using the 1-Ethyl-3-methylimidazolium Acetate ([emim][CH_3COO]) Ionic Liquid. *J. Phys. Chem. B* **2012**, *116*, 283−295.
(35) Nulwala, H. B.; Tang, C. N.; Kail, B. W.; Damodaran, K.; Kaur, P.; Wickramanayake, S.; Shi, W.; Luebke, D. R. Probing the Structure-Property Relationship of Regioisomeric Ionic Liquids with Click Chemistry. *Green Chem.* **2011**, *13*, 3345−3349.
(36) Goodrich, B. F.; de la Fuente, J. C.; Gurkan, B. E.; Lopez, Z. K.; Price, E. A.; Huang, Y.; Brennecke, J. F. Effect of Water and Temperature on Absorption of CO_2 by Amine-Functionalized Anion-Tethered Ionic Liquids. *J. Phys. Chem. B* **2011**, *115*, 9140−9150.
(37) Shi, W.; Damodaran, K.; Nulwala, H. B.; Luebke, D. R. Theoretical and Experimental Studies of Water Interaction in Acetate Based Ionic Liquids. *Phys. Chem. Chem. Phys.* **2012**, *14*, 15897−15908.
(38) Thompson, R. L.; Shi, W.; Albenze, E.; Kusuma, V. A.; Hopkinson, D.; Damodaran, K.; Lee, A. S.; Kitchin, J. R.; Luebke, D. R.; Nulwala, H. Probing the Effect of Electron Donation on CO_2 Absorbing 1,2,3-trizolide Ionic Liquids. *RSC Adv.* **2014**, *4*, 12748−12755.
(39) Allen, M. P.; Tildesley, D. J. *Computer Simulation of Liquids*; Clarendon: Oxford, U.K., 1987.
(40) Cadena, C.; Maginn, E. J. Molecular Simulation Study of Some Thermophysical and Transport Properties of Triazolium-Based Ionic Liquids. *J. Phys. Chem. B* **2006**, *110*, 18026−18039.
(41) Wu, X.; Liu, Z.; Huang, S.; Wang, W. Molecular Dynamics Simulation of Room-Temperature Ionic Liquid Mixture of [bmim]-[BF_4] and Acetonitrile by a Refined Force Field. *Phys. Chem. Chem. Phys.* **2005**, *7*, 2771−2779.
(42) Shi, W.; Maginn, E. J. Atomistic Simulation of the Absorption of Carbon Dioxide and Water in the Ionic Liquid 1-n-hexyl-3-methylimidazolium bis(trifluoromethylsulfonyl) imide ([hmim]-[Tf_2N]). *J. Phys. Chem. B* **2008**, *112*, 2045−2055.
(43) Joung, I. S.; Cheatham, T. E., III. Determination of Alkali and Halide Monovalent Ion Parameters for Use in Explicitly Solvated Biomolecular Simulations. *J. Phys. Chem. B* **2008**, *112*, 9020−9041.
(44) Zhao, X.; Chen, B.; Karaborni, S.; Siepmann, J. Vapor-Liquid and Vapor-Solid Phase Equilibria for United-Atom Benzene Models Near Their Triple Points: The Importance of Quadrupolar Interactions. *J. Phys. Chem. B* **2005**, *109*, 5368−5374.
(45) Vanommeslaeghe, K.; Hatcher, E.; Acharya, C.; Kundu, S.; Zhong, S.; Shim, J.; Darian, E.; Guvench, O.; Lopes, P.; Vorobyov, I.; et al. CHARMM General Force Field: A Force Field for Drug-Like Molecules Compatible with the CHARMM All-Atom Additive Biological Force Fields. *J. Comput. Chem.* **2010**, *31*, 671−690.
(46) Frisch, M. J.; Trucks, G. W.; Schlegel, H. B.; Scuseria, G. E.; Robb, M. A.; Cheeseman, J. R.; Scalmani, G.; Barone, V.; Mennucci, B.; Petersson, G. A.; et al. *Gaussian 09*, revision A.1; Gaussian, Inc.: Wallingford, CT, 2009.
(47) Senapati, S.; Berkowitz, M. Molecular Dynamics Simulation Studies of Polyether and Perfluoropolyether Surfactant Based Reverse Micelles in Supercritical Carbon Dioxide. *J. Phys. Chem. B* **2003**, *107*, 12906−12916.
(48) Phillips, J. C.; Braun, R.; Wang, W.; Gumbart, J.; Tajkhorshid, E.; Villa, E.; Chipot, C.; Skeel, R. D.; Kale, L.; Schulten, K. Scalable Molecular Dynamics with NAMD. *J. Comput. Chem.* **2005**, *26*, 1781−1802.
(49) Shi, W.; Maginn, E. J. Continuous Fractional Component Monte Carlo: An Adaptive Biasing Method for Open System Atomistic Simulations. *J. Chem. Theory Comput.* **2007**, *3*, 1451−1463.
(50) Shi, W.; Sorescu, D. C.; Luebke, D. R.; Keller, M. J.; Wickramanayake, S. Molecular Simulations and Experimental Studies of Solubility and Diffusivity for Pure and Mixed Gases of H_2, CO_2, and Ar Absorbed in the ionic liquid 1-n-Hexyl-3-methylimidazolium Bis(Trifluoromethylsulfonyl)amide ([hmim][Tf_2N]). *J. Phys. Chem. B* **2010**, *114*, 6531−6541.
(51) Cotts, R.; Hoch, M.; Sun, T.; Markert, J. Pulsed Field Gradient Stimulated Echo Methods for Improved NMR Diffusion Measurements in Heterogeneous Systems. *J. Magn. Reson.* **1989**, *83*, 252−266.
(52) Wu, D.; Chen, A.; Johnson, C. An Improved Diffusion-Ordered Spectroscopy Experiment Incorporating Bipolar-Gradient Pulses. *J. Magn. Reson., Ser. A* **1995**, *115*, 260−264.
(53) Stejskal, E.; Tanner, J. Spin Diffusion Measurements: Spin Echoes in the Presence of a Time-Dependent Field Gradient. *J. Chem. Phys.* **1965**, *42*, 288−292.
(54) Tanner, J. Use of Stimulated Echo in NMR-Diffusion Studies. *J. Chem. Phys.* **1970**, *52*, 2523−2526.
(55) Li, Y.; Ye, H.; Zeng, P.; Qi, F. Volumetric Properties of Binary Mixtures of the Ionic Liquid 1-Butyl-3-Methylimidazolium Tetrafluoroborate with Aniline. *J. Solution Chem.* **2010**, *39*, 219−230.
(56) Jacquemin, J.; Husson, P.; Mayer, V.; Cibulka, I. High-Pressure Volumetric Properties of Imidazolium-Based Ionic Liquids: Effect of the Anion. *J. Chem. Eng. Data* **2007**, *52*, 2204−2211.
(57) Machida, H.; Taguchi, R.; Sato, Y.; Smith, R. L., Jr. Measurement and Correlation of High Pressure Densities of Ionic Liquids, 1-Ethyl-3-methylimidazolium L-Lactate ([emim][Lactate]), 2-Hydroxyethyl-trimethylammonium L-Lactate ([$(C_2H_4OH)(CH_3)_3N$-[Lactate]), and 1-Butyl-3-methylimidazolium Chloride ([bmim][Cl]). *J. Chem. Eng. Data* **2011**, *56*, 923−928.
(58) Govinda, V.; Attri, P.; Venkatesu, P.; Venkateswarlu, P. Thermophysical Properties of Dimethylsulfoxide with Ionic Liquids at Various Temperatures. *Fluid Phase Equilib.* **2011**, *304*, 35−43.
(59) NIST Web Book. http://webbook.nist.gov/cgi/cbook.cgi?Contrib=LMF; accessed Oct 1, 2013.
(60) Falcone, D. R.; Douglass, D. C.; McCall, D. W. Self-Diffusion in Benzene. *J. Phys. Chem.* **1967**, *71*, 2754−2755.
(61) Yan, T. Y.; Burnham, C. J.; Pópolo, M. G. D.; Voth, G. A. Molecular Dynamics Simulation of Ionic Liquids: The Effect of Electronic Polarizability. *J. Phys. Chem. B* **2004**, *108*, 11877−11881.
(62) Sarraute, S.; Gomes, M. F. C.; Padua, A. A. H. Diffusion Coefficients of 1-Alkyl-3-methylimidazolium Ionic Liquids in Water, Methanol, and Acetonitrile at Infinite Dilution. *J. Chem. Eng. Data* **2009**, *54*, 2389−2394.
(63) Shiflett, M. B.; Yokozeki, A. Solubilities and Diffusivities of Carbon Dioxide in Ionic Liquids: [bmim][PF_6] and [bmim][BF_4]. *Ind. Eng. Chem. Res.* **2005**, *44*, 4453−4464.
(64) Kroon, M.; Shariati, A.; Costantini, M.; van Spronsen, J.; Witkamp, G.; Sheldon, R.; Peters, C. High-Pressure Phase Behavior of Systems with Ionic Liquids: Part V. The Binary System Carbon Dioxide+1-butyl-3-methylimidazolium Tetrafluoroborate. *J. Chem. Eng. Data* **2005**, *50*, 173−176.
(65) Jang, S.; Cho, D.; Im, T.; Kim, H. High-Pressure Phase Behavior of CO_2 + 1-butyl-3-methylimidazolium Chloride System. *Fluid Phase Equilib.* **2010**, *299*, 216−221.